Journal of Sailing Technology 2023, volume 8, issue 1, pp. 183-199.
The Society of Naval Architects and Marine Engineers.

Boundary Element Method Analysis of 3D Effects and Free-Surface Proximity on Hydrofoil Lift and Drag Coefficients in Varied Operating Conditions

Hugo Nicolas
IRENav, École Navale, Brest, France.

Paolo Perali
IRDL, CNRS UMR 6027, ENSTA Bretagne, Brest, France.

Matthieu Sacher
IRDL, CNRS UMR 6027, ENSTA Bretagne, Brest, France.

Patrick Bot
IRENav, École Navale, Brest, France, patrick.bot@ecole-navale.fr.

Manuscript received July 10, 2023; revision received November 12, 2023; accepted November 25, 2023.

Abstract. The use of hydrofoils to enhance ship performance raises the scientific issue of free-surface proximity, which is important to consider during the design stage, to feed velocity prediction programs, for instance. Typically, the flow over a shallowly submerged hydrofoil is characterized by the Froude number, the submergence depth-to-chord ratio, the angle of attack, and geometric parameters of the lifting surface. Among these parameters, the present paper investigates the influence of the wing aspect ratio on the lift and drag coefficients of hydrofoils operating near a free surface. For this purpose, rectangular wings with an H105 profile at 2° angle of attack and aspect ratios ranging from 4 to 20 are systematically analyzed using a 3D boundary element method. The free surface is modeled using a linearized Neumann-Kelvin boundary condition. Chord-based Froude numbers of 0.5, 1.1, and 6.3 are studied. The submersion depth is swept between 0.1 and 30 times the foil chord length. The evolution of the normalized lift and drag coefficients with respect to the foil submersion and the aspect ratio is discussed in detail. Flow velocity is shown to play a significant role in the evolution of the lift and drag coefficients with submersion depth, close to the free surface, for all the aspect ratios. Its influence gets reduced by moving away from the free surface. The critical submersion depth, where the free-surface effects cease, is found to increase with higher flow velocity and aspect ratio. Furthermore, both positive and negative correlations between the force coefficients and the aspect ratio are identified, depending on the operating conditions. It is found that when the proximity to the free surface either enhances or impairs a force coefficient relative to its value in unbounded flow, increasing the aspect ratio amplifies this effect. Overall, this study confirms the effectiveness of steady boundary element methods for simulating the flow around hydrofoil wings in the vicinity of a free surface and contributes to further understanding the influence of geometric parameters on hydrofoil performance.

Keywords: hydrofoil; free surface; aspect ratio; potential flow; boundary element method (BEM).

NOMENCLATURE

c	Hydrofoil chord length [m]
C_D	Drag coefficient [–]
$C_{D\infty}$	Drag coefficient in unbounded flow [–]
C_L	Lift coefficient [–]
$C_{L\infty}$	Lift coefficient in unbounded flow [–]
Fr	Froude number [–]
Fr_c	Chord-based Froude number ($Fr_c = U_0/\sqrt{gc}$) [–]
g	Gravitational acceleration [m s^{-2}]
h	Submergence depth [m]
$\boldsymbol{n}$	Vector normal to the domain boundary [m]
r	Distance to velocity potential [m]
S	Surface of the domain boundary [m^2]
S_B	Body surface of the domain boundary [m^2]
S_{FS}	Free surface of the domain boundary [m^2]
S_W	Wave surface of the domain boundary [m^2]
$\boldsymbol{u}$	Velocity field vector [m s^{-1}]
U_0	Undisturbed flow velocity in the x-direction [m s^{-1}]
$\boldsymbol{U_0}$	Undisturbed flow velocity vector [m s^{-1}]
(x, y, z)	Cartesian coordinate system [m]

α	Hydrofoil angle of attack [°]
η	Free-surface elevation [m]
Λ	Wing aspect ratio [–]
μ	Doublet strength [m s^{-1}]
σ	Source strength [m^2 s^{-1}]
ϕ	Perturbation velocity potential [m^2 s^{-1}]

BEM	Boundary element method
LLT	Lifting line theory
RANS	Reynolds-average Navier-Stokes
VLM	Vortex lattice method
VPP	Velocity prediction program

1 INTRODUCTION

Hydrofoils enhance the performance of marine vehicles, including sailboats and commercial ships, by reducing hydrodynamic resistance and improving seakeeping. Whether partially submerged or fully submerged, these appendages often operate close to the water's surface. Their proximity to the free surface is a critical factor to consider in the design stage (Bal, 2007), as recently demonstrated through the implementation of a velocity prediction program (VPP) for the America's Cup AC50 and AC75 yachts (Patterson and Binns, 2022). Yet, the complex physics involved is challenging to capture. The tools available for addressing the free-surface problem consist of simulations of varying fidelity levels, including methods such as lifting-line theory (LLT), vortex lattice method (VLM), panel method, and Reynolds-averaged Navier-Stokes (RANS) solvers, as well as experimental approaches. When it comes to simulations, the choice of fidelity level often results from a trade-off between computational efficiency and model accuracy.

Previous studies have observed that the proximity to the free surface alters the flow field compared to unbounded flow, which can significantly impact hydrofoil performance (Zhu et al., 2006). Specifically, the low pressure on the suction side of a lifting surface acts to deform the free surface, resulting in the

generation of transverse waves whose characteristics are dictated by the flow regime (Parkin et al., 1955). Parkin et al. (1955) further illustrated that the presence of a free surface leads to two distinct flow regimes, corresponding to low and high chord-based Froude numbers (Fr_c). Therefore, the Froude number (Fr) emerges as a dominant parameter in the problem, alongside the submergence depth-to-chord ratio (h/c), and other parameters such as the angle of attack (α) (Kwag and Mori, 1991).

The aforementioned transition in the wave patterns between low and high Froude numbers has been extensively documented in the scientific literature, primarily on 2D profiles (Bai, 1978; Yasko, 1998; Chen, 2012; Carabineanu, 2014). At high Froude numbers, a smooth transverse wave forms above the foil, significantly diminishing lift as the body nears the free surface (Daskovsky, 2000). In contrast, low Froude numbers disrupt the free surface by gravity waves and hydraulic jumps (Parkin et al., 1955). In this flow regime, the flow behavior depends on both the submergence depth-to-chord ratio and the Froude number. In close proximity to the free surface, a standing wave crest can manifest slightly ahead of the foil, with another crest further aft along the chord, resulting in a decrease in lift (Laitone, 1954; Pernod et al., 2023). Increasing the submersion depth increases the wavelength (Karim et al., 2014). Uddin and Karim (2017) have also demonstrated that the wave amplitude is influenced by the submergence depth, with increased steepness as the free surface is approached, potentially leading to wave-breaking (Duncan, 1983). In cases of wave-breaking, unsteady breaking waves introduce fluctuations in both lift and drag (Prasad et al., 2015). By further reducing the Froude number, the free surface behaves akin to a rigid wall (Faltinsen, 2005). In such instances, flow acceleration occurs above the suction side of the hydrofoil, analogous to a ground effect (Giesing and Smith, 1967). Consequently, hydrofoil lift increases until a critical value of h/c is reached, above which it rapidly diminishes when approaching too close to the free surface (Filippas and Belibassakis, 2014).

The variation of the lift coefficient (C_L) with the Froude number is characteristic of the challenge posed by the free-surface proximity. The impact of the alterations in the wave patterns between low and high Froude numbers on the lift coefficient was demonstrated by Yeung and Bouger (1979) through a hybrid integral-equation method. The analyses conducted by Yeung and Bouger (1979) have since served as benchmarks for validating numerical models for 2D and 3D hydrofoils operating beneath a free surface (Bal, 1999; Bal et al., 2001). Kennell and Plotkin (1984) additionally noted that the lift coefficient attains its maximum value when operating at a low Froude number in proximity to $h/c = 1$, as observed in their case. Furthermore, Hough and Moran (1969) reported that the lift coefficient remains nearly constant above a chord-based Froude number of 10. Consequently, Hough and Moran (1969) designated the range of interest for high-speed operating conditions as $Fr_c \in [3 - 10]$.

Concerning drag, a peak in the drag coefficient is observed in close proximity to the free surface, with respect to h/c (Bal et al., 2001). This peak's occurrence is independent of the flow regime, but its magnitude decreases with increasing flow velocity (Xie and Vassalos, 2007). The significance of drag mitigation due to flow velocity is underscored by Plotkin's observation that the drag coefficient (C_D) experiences significant damping at low Froude numbers (Plotkin, 1975). Ultimately, the influence of the free-surface proximity on the lift and drag coefficients diminishes above a specific submergence threshold (Ali and Karim, 2010). Above this threshold, the submersion depth can be regarded as effectively infinite (Hoque et al., 2017).

Regarding the impact of the angle of attack on the hydrodynamic characteristics of shallowly submerged hydrofoils, the lift coefficient follows a linear progression with the angle of attack (until reaching stall), similar to the behavior observed in unbounded flow (Wadlin et al., 1952; Binns et al., 2008). Ni et al. (2021) demonstrated that motion-induced surface waves can enhance hydrofoil performance by delaying stall, particularly at high angles of attack. Moreover, the evolution of the drag coefficient exhibits a quadratic relationship with respect to the lift coefficient, as discussed by Binns et al. (2008).

Binns et al. (2008) also revealed that increasing the heel angle does not impair the lift-to-drag ratio of a full T-foil and highlighted ventilation inception under extreme sailing conditions, characterized by α, h/c, and Fr_c.

As for hydrofoil geometry, early studies on its impact on the hydrodynamic characteristics employed a lifting-line approach (Michel et al., 1954). More recently, an iterative BEM developed by Bal and Kinnas (2002) was used for investigating the effects of curved wing tips and taper ratio on the performance of 3D shallowly submerged cavitating hydrofoils under various operating conditions at chord-based Froude numbers up to 1.6 and 0.8, respectively (Bal, 2023a; Bal, 2023b). These studies have highlighted the considerable influence of hydrofoil geometry in the context of free-surface proximity.

Among the typical parameters describing the geometry of lifting surfaces, there remains limited knowledge concerning the influence of the wing aspect ratio (Λ) on the performance of hydrofoils near a free surface, as no thorough investigation into its influence over a broad range of varied operating conditions was conducted. Thiart (1997) developed a VLM for finite-span hydrofoil wings operating beneath a free surface to explore the effects of aspect ratio, taper ratio, sweep angle, and dihedral angle on hydrofoil lift and drag. Thiart (2001) focused on rectangular wings with aspect ratios up to 10 under fixed operating conditions, with the exception of the chord-based Froude number, which ranged from 0 to 20. In a separate study, a panel method was employed to compute the lift coefficient for foils with aspect ratios of 4, 5, and 6 at low Froude numbers and a submergence depth-to-chord ratio of 1 (Xie and Vassalos, 2007). Using a similar level of fidelity, Ozdemir et al. (2021) assessed the wave field and hydrodynamic performance of shallowly submerged hydrofoils with aspect ratios ranging from 4 to 8, operating at low and moderate Froude numbers and with h/c equal to 0.75, 1, and 1.5. The comparisons between 2D and 3D cases revealed that, although performance tends to improve with increasing aspect ratio, the behavior of shallowly submerged 3D hydrofoils can differ significantly from that of their 2D counterparts, depending on the Froude number.

Therefore, a gap remains in the understanding of the effects of the aspect ratio on the performance of submerged hydrofoils, particularly at high Froude numbers ($Fr_c > 3$) commonly encountered in practical foiling scenarios. Thus, this paper introduces a method to explore how the wing aspect ratio and the submersion depth affect the lift and drag coefficients of hydrofoils operating at low, moderate, and high Froude numbers. Section 2 outlines the methodology and establishes the numerical framework, which consists of modeling and meshing wing geometries with different aspect ratios, and solving the fluid problem for different Froude numbers and submersion depths, using a 3D BEM approach. Section 3 details the numerical setup. In Section 4, the numerical framework is applied to the parametric case studies. The lift and drag coefficients computed for each wing, under each operating condition, are analyzed with respect to submersion depth and aspect ratio.

2 NUMERICAL FRAMEWORK

2.1 Problem Formulation

Figure 1 provides a descriptive representation of the flow around a shallowly submerged hydrofoil. In Figure 1, U_0 is the flow velocity in the x-direction and η is the free-surface elevation. The submersion depth is defined at the mid-chord of the centerline, coinciding with the center of rotation of the angle of attack. The submergence depth-to-chord ratio is defined between this point and the free surface at rest, $z = 0$.

2.2 Geometry Modeling and Meshing

The appendages were generated using *LEModeler* (https://github.com/hugo-nicolas/LEModeler), an open-source code for modeling parametric hydrofoil geometries developed for the purpose of this study, using the *Rhinoceros*® CAD engine. The geometries were meshed using structured grids refined at both the leading and trailing edges. To capture the 3D effects, the spanwise panel distribution

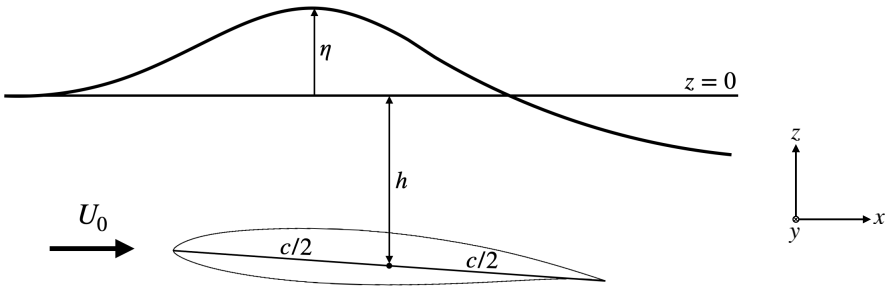

Figure 1. Schematic description of the fluid problem.

was refined to leave smaller square cells at the foil tips.

2.3 Hydrodynamic Model

The fluid problem was addressed using *PUFFIn* (https://www.ensta-bretagne.fr/fr/optifoil), a 3D potential flow solver based on a BEM approach. The solver *PUFFIn* is detailed in Perali et al. (2022) and the theoretical framework for steady simulations used in the present work is summarized here.

The fluid flow is considered incompressible and irrotational, and viscous effects are neglected. The velocity field ($\boldsymbol{u}$) is the superposition of the undisturbed velocity ($\boldsymbol{U_0}$) with the gradient of the perturbation potential (ϕ). It satisfies Laplace's equation,

$$\boldsymbol{\nabla}^2\phi = 0. \tag{1}$$

Applying the second Green identity to this equation yields the boundary integral equation (Katz and Plotkin, 2001),

$$\phi = -\frac{1}{4\pi}\int_S \left[\sigma\frac{1}{r} - \mu\,\boldsymbol{n}\cdot\boldsymbol{\nabla}\left(\frac{1}{r}\right)\right]\mathrm{d}S, \tag{2}$$

where σ is the source strength and μ is the doublet strength such that

$$\sigma = -\frac{\partial\phi}{\partial n}, \quad \mu = -\phi. \tag{3}$$

S is the domain boundary, which typically consists of the body surface (S_B), the wake surface (S_W), and the free-surface boundary (S_{FS}). $\boldsymbol{n}$ is the outward pointing vector normal to S. Under the assumption that the wake should not support hydrodynamic loads, the source distribution on the wake surface is null. Consequently, Equation 2 can be rewritten as

$$\phi = -\frac{1}{4\pi}\int_{S_B+S_{FS}} \left[\sigma\frac{1}{r} - \mu\,\boldsymbol{n}\cdot\boldsymbol{\nabla}\left(\frac{1}{r}\right)\right]\mathrm{d}S + \frac{1}{4\pi}\int_{S_W}\left[\mu\,\boldsymbol{n}\cdot\boldsymbol{\nabla}\left(\frac{1}{r}\right)\right]\mathrm{d}S, \tag{4}$$

with the source strength given by the non-penetration condition on the hydrofoil,

$$\sigma = -\boldsymbol{U_0}\cdot\boldsymbol{n}. \tag{5}$$

PUFFIn models the free surface using either a linearized Neumann-Kelvin, a symmetry condition, or an antisymmetry boundary condition. The symmetry and antisymmetry boundary conditions result from the asymptotic behaviors of the Froude number $Fr \longrightarrow 0$ and $Fr \longrightarrow \infty$, respectively (Newman, 2018). In the scope of this paper, the simulations were run using the Neumann-Kelvin formulation linearized at $z = 0$,

$$(\boldsymbol{U_0} \cdot \boldsymbol{\nabla})^2 \, \phi + g \frac{\partial \phi}{\partial z} = 0, \tag{6}$$

where g is the gravitational acceleration.

To solve the problem numerically, the boundaries are discretized using quadrilateral elements. The distribution of sources and doublets is assumed constant on each element. Writing Equation 4 at the geometric center of each element yields the general matrix form (Filippas and Belibassakis, 2014)

$$\boldsymbol{A}(\eta) \begin{bmatrix} \boldsymbol{\mu_B} \\ \\ \boldsymbol{\sigma_{FS}} \end{bmatrix} = \boldsymbol{B}(\eta) \begin{bmatrix} \boldsymbol{\sigma_B} \\ \\ \boldsymbol{\mu_{FS}} \end{bmatrix} + \boldsymbol{W}(\eta) \, \boldsymbol{\mu_W}, \tag{7}$$

where the free-surface elevation is given by

$$\eta = -\frac{1}{g} \, \boldsymbol{U_0} \cdot \boldsymbol{\nabla} \phi. \tag{8}$$

$\boldsymbol{\sigma_B}$ and $\boldsymbol{\mu_B}$ denote the strengths of sources and doublets on the body, respectively. Similarly, $\boldsymbol{\sigma_{FS}}$ and $\boldsymbol{\mu_{FS}}$ represent the strengths of sources and doublets on the free surface. $\boldsymbol{\mu_W}$ corresponds to the doublet strengths on the wake panels. $\boldsymbol{\sigma_B}$ is determined by Equation 5 while the other strength vectors are unknown. $\boldsymbol{A}(\eta)$, $\boldsymbol{B}(\eta)$, and $\boldsymbol{W}(\eta)$ can be computed for constant-strength singularity panels. Considering the linearized free-surface boundary condition 6, the problem is solved by inverting $\boldsymbol{A}(\eta)$ once at the beginning of the computation, using a lower-upper decomposition.

A Lagrangian approach is employed to construct the wake surface during the computation. This process is iterative in time, meaning that the position of a wake panel at the current time step is determined based on the velocity values from the previous time step. Since the flow is considered inviscid, the potential on a wake panel convected by the flow remains constant. Thus, $\boldsymbol{\mu_W}$ only depends on the strengths of the doublets on the panels located downstream of the trailing edge, which are computed by imposing pressure equality between the suction side and the pressure side, known as the Kutta condition, at the trailing edge of the hydrofoil.

The pressure distribution on the body is yielded by the Bernoulli relation. From there, the hydrodynamic forces and moments acting on the hydrofoil are computed by integrating the pressure over the body surface. The simulations end when a residual criterion on the last N iterations is met.

2.4 Remarks on the Hydrodynamic Model

The numerical model applies to steady simulations. As noted by Prasad et al. (2015), wave-breaking may occur at low submergence, leading to unsteadiness and fluctuations in both lift and drag. However, since *PUFFIn* considers inviscid and irrotational flow, it does not capture this phenomenon. Additionally, unsteadiness in the wake of the hydrofoil can arise in close proximity to the free surface,

particularly at low Froude numbers. Extremely close proximity to the free surface can result in significant changes in wave steepness, affecting hydrofoil immersion and making the convergence of the simulations more challenging. Most importantly, the model does not consider multiphase flow phenomena like cavitation or ventilation, which limits the ability to draw quantitative conclusions at very low immersion levels. Therefore, this paper does not provide conclusions for these extreme operating conditions. Nevertheless, despite these limitations, the results presented in Section 4 offer qualitative insights into the evolution of the lift and drag coefficients in the vicinity of the free surface, aligning with observations in the existing literature.

3 NUMERICAL SETUP

3.1 Numerical Parameters

The numerical framework was applied to hydrofoil wings with an aspect ratio of 4, 6, 10, and 20, operating at different Froude numbers and submersion depths. In particular, three chord-based Froude numbers equal to 0.5, 1.1, and 6.3 were analyzed. They respectively correspond to a low, moderate, and high Froude number. The lifting surfaces were modeled rectangular to avoid accumulating effects induced by more complex geometries and rather focus on the influence of the aspect ratio. Their chord length was fixed to 0.125 m. Consequently, each Froude number corresponds to a given flow velocity, and the changes in the aspect ratio were achieved by adjusting the wing span. The angle of attack remained constant and equal to $+2^\circ$. The cross-section profile was an H105 profile (Speer, 2001), which is close to most sections used in foil design. Thus, the zero-lift angle of attack was -2.35°. Concerning submersion depth, a wide range of submergence depth-to-chord ratios between 0.1 and 30 were swept. Water density was assumed constant and equal to 1025 kg/m^3. Finally, an infinite depth of water was considered to avoid the effects of shallow water. The operating conditions investigated in this paper are summarized in Table 1.

Table 1. Operating conditions investigated.

Fr_c [–]	U_0 [m s^{-1}]	α [°]	h/c [–]
0.5	0.6	2	0.1−30
1.1	1.2	2	0.1−30
6.3	7.0	2	0.1−30

The size of the free surface domain was determined by the foil's chord length. Upstream of the foil was left a distance of 5 chords while downstream of the foil was left 40 chord lengths. Port and starboard, the distance to the foil tips was 20 times the chord length such that the hydrofoil was centered in the transverse direction of the flow. The residual criterion for stopping the hydrodynamic simulations was defined such that the maximum deviation on the forces is 0.005 N for the last $N = 20$ iterations.

3.2 Mesh Convergence Study

The mesh topology was first established on the hydrofoil with an aspect ratio of 4 and further adapted to the lifting surfaces of higher aspect ratios while keeping the same mesh topology as $\Lambda = 4$. For this reason, the mesh convergence analysis was conducted on the wing with an aspect ratio of 4. The convergence study was conducted at a Froude number of 6.3 and a submergence depth-to-chord ratio of 20. The results of the mesh convergence study on the lift coefficient are shown in Figure 2. To balance cost and accuracy, the mesh of 1280 panels (16 panels spanwise and 40 along the chord on each side) was selected as the reference. Figure 3 shows a 3D view of the reference geometry.

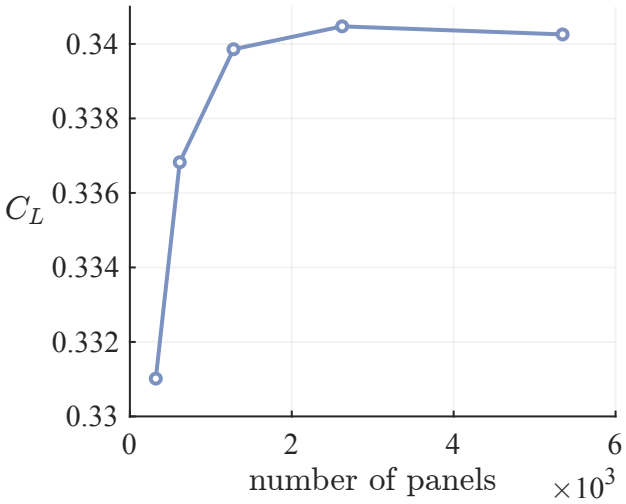

Figure 2. Mesh convergence on the lift coefficient for the wing with an aspect ratio of 4. The chord-based Froude number is 6.3 and the submergence depth-to-chord ratio equals 20.

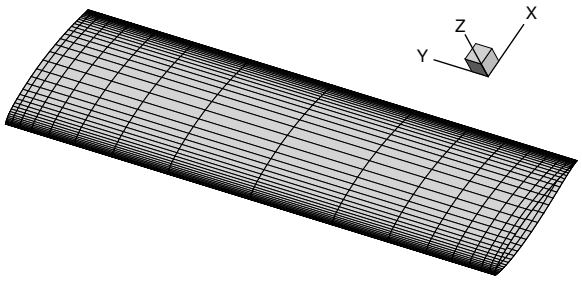

Figure 3. Selected mesh for the wing with an aspect ratio of 4.

4 RESULTS

4.1 Influence of the Free-Surface Proximity

The lift and drag coefficients computed for each wing, under each operating condition in Table 1, were normalized by their respective value in unbounded flow ($C_{L\infty}$ and $C_{D\infty}$). The results of these simulations are presented in Figure 4, with Figure 4 (a), (b), and (c) showing the normalized lift coefficient, and Figure 4 (d), (e), and (f) the normalized drag coefficient with respect to the submergence depth-to-chord ratio. The trends observed in Figure 4 are contextualized within the existing literature.

In Figure 4 (a), (b), and (c), the lift coefficient plummets when approaching too close to the free surface, no matter the flow velocity. As discussed in Section 2.4, the values of the force coefficients in close proximity to the free surface (typically $h/c < 0.5$ here) must be taken with caution since unsteadiness may occur. Nevertheless, the significant reduction in the lift coefficient observed in the present work is in agreement with the literature, giving confidence in the use of steady BEM to provide an overview of hydrofoil performance near the free surface (Chen, 2012).

Figure 4 (a), (b), and (c) illustrates that the characteristic evolution of the lift coefficient between low and high Froude numbers is well captured by the simulations. Notably, a portion of the normalized lift coefficient exceeds 1 for the chord-based Froude numbers 0.5 and 1.1. The occurrence of such a gain in the lift coefficient was also identified in other studies at low Froude numbers (Pernod et al., 2023). Figure 4 (a) exhibits that, in the present work, this gain in the lift coefficient occurs near $h/c = 1$ at the chord-based Froude number of 0.5. It enhances the lift coefficient by up to 15.8 % compared to its value in unbounded flow for the wing with an aspect ratio of 20, which suggests a potential benefit of operating in the vicinity of the free surface for maximizing the lift coefficient, under specific operating conditions. Figure 4 (b) illustrates that the amplitude of the gain is smaller at $Fr_c = 1.1$ than at $Fr_c = 0.5$. The gain also occurs at a greater h/c compared to $Fr_c = 0.5$, close to $h/c = 3$ for the larger wings. At the chord-based Froude number of 6.3, it is made clear from Figure 4 (c) that the gain in the lift coefficient has disappeared completely. Therefore, the proximity to the free surface systematically reduces the lift coefficient at the higher Froude number, which is consistent with other studies when inertial forces largely dominate (Daskovsky, 2000).

Figure 4 (d) shows that, at the chord-based Froude number of 0.5, the normalized drag coefficient first decreases before peaking by approaching the free surface. A similar behavior may be observed at the intermediate Froude number in Figure 4 (e), with a noticeable reduction in the drag coefficient

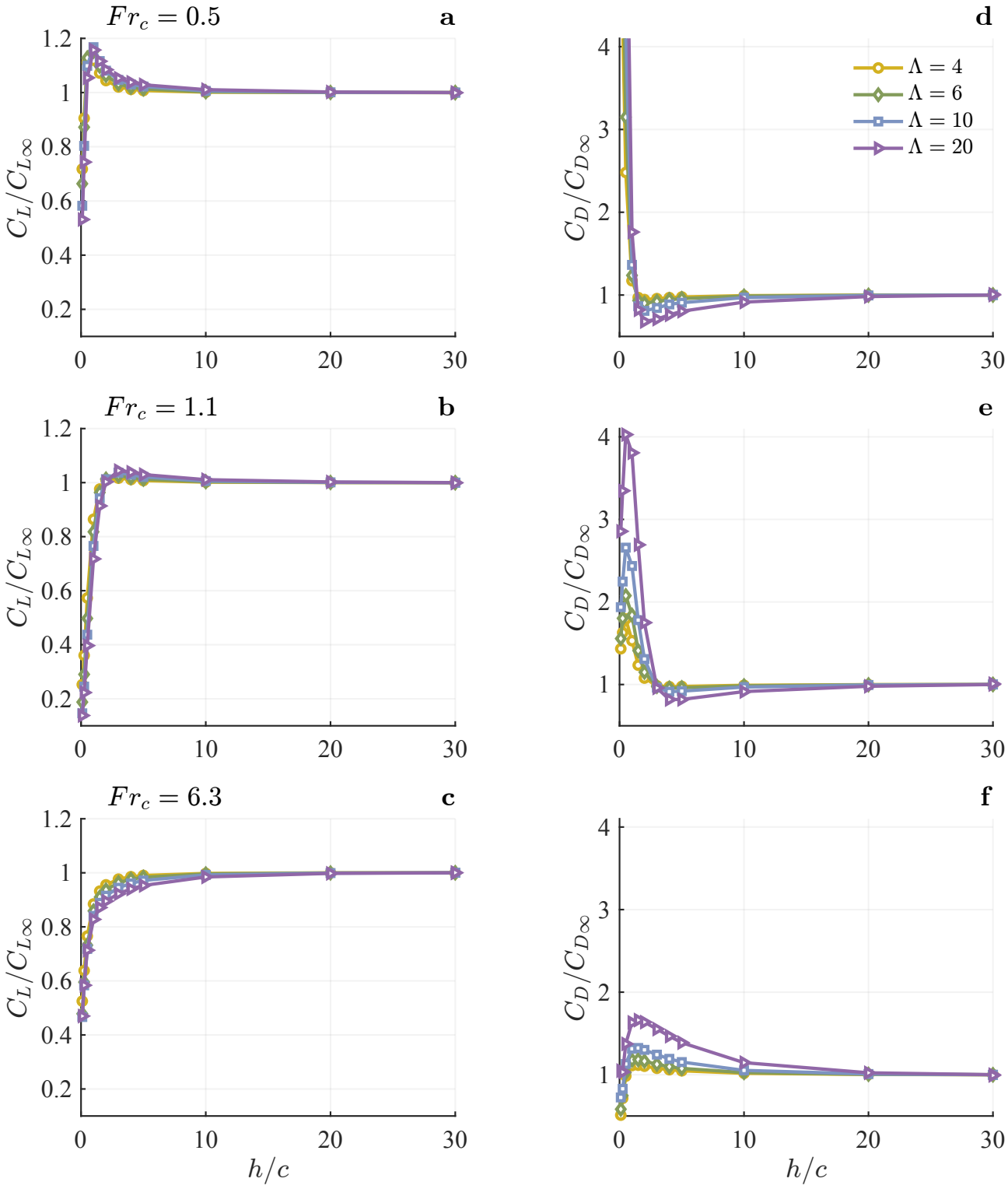

Figure 4. Evolution of the normalized lift and drag coefficients with the submergence depth-to-chord ratio for different wing aspect ratios and chord-based Froude numbers.

for $h/c < 0.5$. The occurrence of the peak preceded by the reduction in the drag coefficient is delayed to greater submergence by increasing the flow velocity. Consequently, Figure 4 (f) shows that the reduction in the drag coefficient common to $Fr_c = 0.5$ and $Fr_c = 1.1$ has disappeared at $Fr_c = 6.3$. Furthermore, the amplitude of the peak is reduced with increasing speed, as shown by Xie and Vassalos (2007).

Figure 4 (a), (b), and (c) illustrates that no matter the aspect ratio, the lift coefficient systematically converges to its value in unbounded flow by increasing h/c. Similar conclusions apply to the drag coefficient based on Figure 4 (d), (e), and (f). In particular, the disappearance of the free-surface effects with increasing h/c is achieved from a threshold value of h/c, whose existence is largely observed in the literature (Hoque et al., 2017). Above this threshold, increasing the aspect ratio increases the lift coefficient and decreases the drag coefficient according to the known effect of the aspect ratio in unbounded flow. Comparing the convergence of the normalized lift and drag coefficients with respect to h/c at each flow velocity reveals that the threshold h/c for achieving behavior akin to infinite submersion depth increases as the chord-based Froude number increases. It is also greater with a larger aspect ratio.

4.2 Influence of the Aspect Ratio

The aspect ratio demonstrates variable effects on the normalized force coefficients in Figure 4, depending on the influence of the free-surface effects on the lift and drag coefficients. These variations include both positive and negative correlations between the aspect ratio and the normalized force coefficients. The characterization of these correlations consists in the main finding of the present work and is discussed below.

Figure 4 (a), (b), and (c) illustrates that increasing the aspect ratio reduces the normalized lift coefficient when $C_L/C_{L\infty} \ll 1$ (negative correlation) and increases it when $C_L/C_{L\infty} \gg 1$ (positive correlation). The same conclusion may be drawn from Figure 4 (d), (e), and (f) for the drag coefficient. Therefore, when the proximity to the free surface either enhances or impairs a force coefficient relative to its value in unbounded flow, increasing the aspect ratio amplifies the effect. This, however, does not appear systematic based on the numerical simulations when the normalized lift and drag coefficients reach a value of 1 under the influence of the free surface.

To provide a clearer representation of the effects of the aspect ratio when the normalized force coefficients approach a value of 1 near the free surface, Figure 5 presents the data from Figure 4 focusing on submergence depth-to-chord ratios up to 4. Figure 5 illustrates the existence of ranges of operating conditions where the correlation between the normalized force coefficients and the aspect ratio is unclear, such as for the lift coefficient at h/c between 0.25 and 2 and $Fr_c = 0.5$. In such instances, the correlation is considered transient. The existence of ranges with transient correlation may result from numerical uncertainties, leading to variations in the results, notably at low Froude numbers.

In light of the changes in the evolution of the normalized lift and drag coefficients versus h/c discussed in Section 4.1, the submersion depth at which the normalized lift and drag coefficients reach a value of 1 increases with the chord-based Froude number. Consequently, the influence of the aspect ratio on the normalized force coefficients is characterized by both the Froude number and the submergence depth-to-chord ratio.

Table 2 (a) and Table 2 (b) respectively summarize the ranges of operating conditions where the correlation between the aspect ratio and the normalized lift and drag coefficients is positive ("$+$"), negative ("$-$"), or transient ("$\longrightarrow$"). Table 2 helped select the test cases shown in Figure 6 to analyze quantitatively the effects of the aspect ratio on the lift and drag coefficients in varied operating conditions.

Figure 6 illustrates how the lift and drag coefficients, normalized by their values in unbounded flow, evolve with the aspect ratio for different submersion depths and chord-based Froude numbers. The

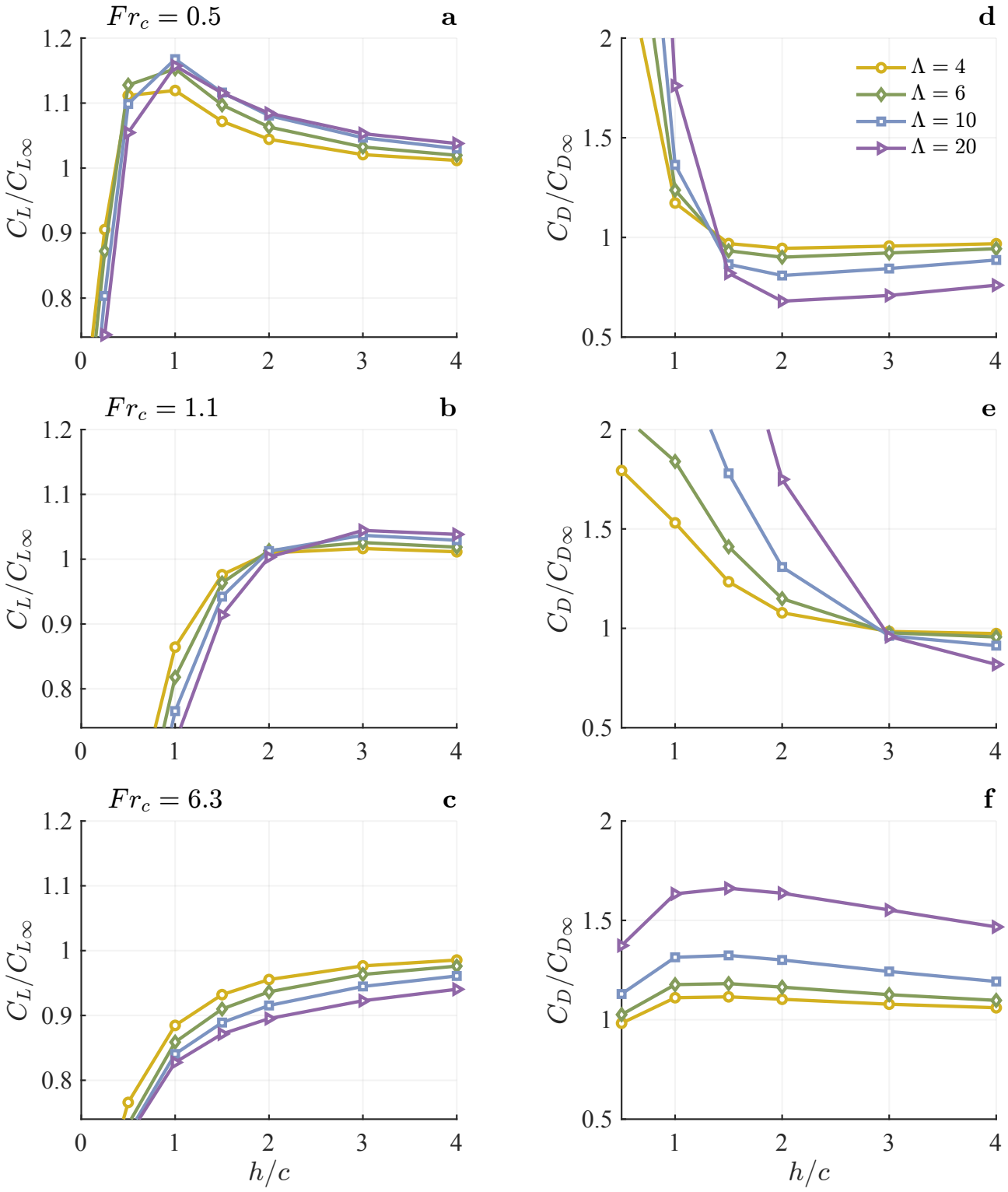

Figure 5. Close-up view of Figure 4 to observe the transient correlations between the force coefficients and the wing aspect ratio across various operating conditions.

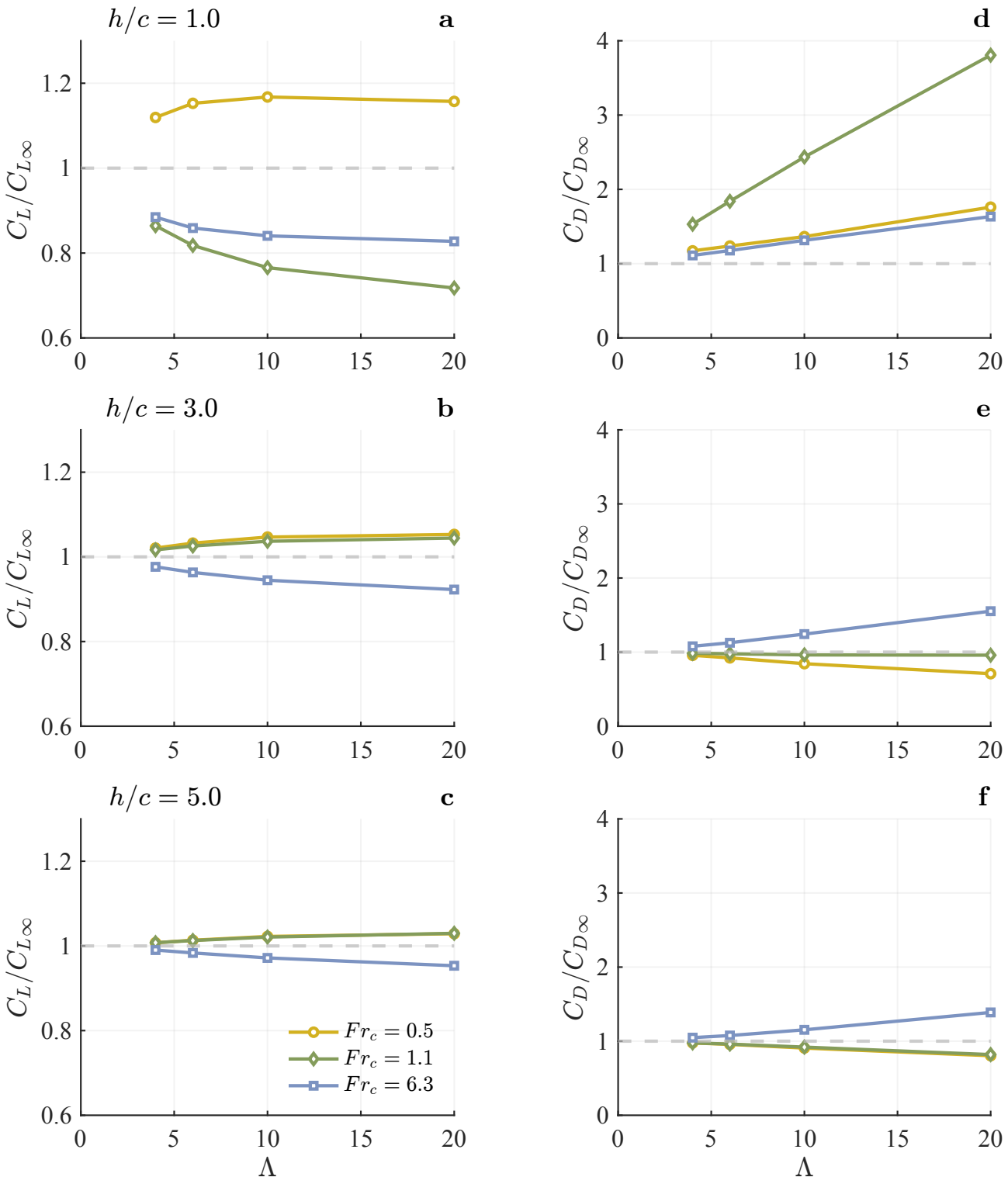

Figure 6. Evolution of the normalized lift and drag coefficients with the wing aspect ratio for different chord-based Froude numbers and submergence depth-to-chord ratios.

Table 2. Summary of the correlations between the wing aspect ratio and the normalized (a) lift coefficient and (b) drag coefficient in varied operating conditions.

(a)

Fr_c	h/c 0.1	0.25	1	1.5	2	3	...	30
0.5	$-$	|	$\longrightarrow$		|		$+$	
1.1	$-$			|	$\longrightarrow$	|	$+$	
6.3				$-$				

(b)

Fr_c	h/c 0.1	0.25	1	1.5	2	3	...	30
0.5	$+$		| $\longrightarrow$ |				$-$	
1.1	$+$				| $\longrightarrow$	|	$-$	
6.3				$+$				

Correlation between a given normalized force coefficient and the aspect ratio:
$-$ negative $+$ positive $\longrightarrow$ transient

submersion depths shown in Figure 6 were selected based on Table 2. Figure 6 (a) and (d) corresponds to $h/c = 1$, where a gain in the normalized lift coefficient was observed in Figure 4 (a). In Figure 6 (a), a negative correlation between the normalized lift coefficient and the aspect ratio can be observed for the chord-based Froude numbers of 1.1 and 6.3. Conversely, a positive correlation between the normalized drag coefficient and the aspect ratio can be observed in Figure 6 (d) for the three Froude numbers. As indicated in Table 2 (a), the correlation between the aspect ratio and the lift coefficient is transient at $h/c = 1$ and $Fr_c = 0.5$, which justifies the non-monotonic evolution of $C_L/C_{L\infty}$ versus Λ for $Fr_c = 0.5$ in Figure 6 (a). The submergence depth-to-chord ratio of 3 was selected as the intermediate case, where the effects of the free surface remain significant yet reduced. At $h/c = 3$, a wing with a larger aspect ratio provides a greater lift coefficient and a smaller drag coefficient, for the chord-based Froude numbers of 0.5 and 1.1. This is shown in Figure 6 (b) and (e), respectively through the positive correlation of the normalized lift coefficient with the aspect ratio and the negative correlation of the drag coefficient with the aspect ratio, at $Fr_c = 0.5$ and $Fr_c = 1.1$. The correlations with the aspect ratio are respectively negative and positive for the normalized lift and drag coefficients, at $Fr_c = 6.3$. Finally, Figure 6 (c) and (f) shows the evolution of the normalized lift and drag coefficients when only a small proportion of the free-surface effects persists. The correlations between the aspect ratio and the force coefficients at $h/c = 5$ are consistent with those observed at $h/c = 3$.

The significant disparity in the lift and drag coefficients at $h/c = 1$ illustrated in Figure 6 (a) and (d) aligns with the observations made in Section 4.1 regarding the significant impact of the Froude number near the free surface. Comparing the evolution of the lift and drag coefficient at each submergence depth-to-chord ratio in Figure 6 reveals that the curves $C_L/C_{L\infty}$ and $C_D/C_{D\infty}$ for $Fr_c = 0.5$ and $Fr_c = 1.1$ tend to superimpose by increasing h/c, for all the aspect ratios analyzed in the present work. Thus, it may be concluded that, for all the aspect ratios, the effects of flow velocity on the lift and drag coefficients decrease and disappear, eventually, by moving away from the free surface.

5 CONCLUSIONS

The present paper investigates the effects of both the free surface and the aspect ratio on the hydrofoil lift and drag coefficients. To do so, simulations on fully submerged rectangular wings of variable aspect ratios under different flow velocities and submersion depths are performed using a 3D boundary

element method with a linearized Neumann-Kelvin boundary condition for the free surface. The difference between low and high Froude numbers is well captured by the flow solver, which demonstrates the applicability of steady panel methods to the problem of fully submerged hydrofoils of variable aspect ratios operating near a free surface.

Several conclusions may be drawn from the present work:

- The threshold submersion depth above which the free-surface effects cease is delayed with both flow velocity and aspect ratio.
- Increasing the aspect ratio can enhance or impair the lift and drag coefficients, depending on the Froude number and the submergence depth-to-chord ratio. When the proximity to the free surface either enhances or impairs a force coefficient relative to its value in unbounded flow, increasing the aspect ratio amplifies this effect.
- At low submergence levels, flow velocity significantly influences the lift and drag coefficients, for all the aspect ratios. Its influence diminishes as immersion depth increases, eventually reaching a point where it becomes negligible.

To provide a comprehensive understanding of the variations in the lift and drag coefficients discussed in this paper, additional analyses of local quantities (such as the pressure coefficients, the free-surface elevation, and the effective angle of attack) are essential. Moreover, investigating the influence of downwash and the transition phenomenon identified in this study should contribute to offering more meaningful and physical interpretations of the results.

Overall, this study contributes to enhancing the understanding of how geometric parameters impact the performance of closely submerged hydrofoils, in view of performing multi-fidelity optimizations, for example.

6 CRediT AUTHORSHIP CONTRIBUTION STATEMENT

Hugo Nicolas: Conceptualization, Methodology, Software, Validation, Formal analysis, Investigation, Writing - Original Draft, Visualization. **Paolo Perali:** Methodology, Software, Validation, Writing - Review & Editing. **Matthieu Sacher:** Conceptualization, Methodology, Writing - Review & Editing, Supervision. **Patrick Bot:** Conceptualization, Resources, Supervision, Project administration, Writing - Review & Editing.

7 ACKNOWLEDGEMENTS

The authors are especially grateful to Galen W. Ng for providing valuable feedback on the manuscript draft.

REFERENCES

Ali, A. and M. Karim (2010). “Numerical Study of Free Surface Effect on the Flow Around Shallowly Submerged Hydrofoil”. In: *Proceedings of MARTEC 2010 The International Conference on Marine Technology*. Vol. 11. Dhaka, Bangladesh, p. 12.

Bai, K. J. (1978). “A Localized Finite-Element Method for Two-Dimensional Steady Potential Flows with a Free Surface”. In: *Journal of Ship Research* 22.04, pp. 216–230. ISSN: 0022-4502. DOI: 10.5957/jsr.1978.22.4.216.

Bal, S. (1999). “A Potential Based Panel Method for 2-D Hydrofoils”. In: *Ocean Engineering* 26.4, pp. 343–361. ISSN: 0029-8018. DOI: 10.1016/S0029-8018(97)10022-1.

Bal, S. (2007). “High-Speed Submerged and Surface Piercing Cavitating Hydrofoils, Including Tandem Case”. In: *Ocean Engineering* 34.14, pp. 1935–1946. ISSN: 0029-8018. DOI: 10.1016/j.oceaneng.2007.03.007.

Bal, S. (2023a). “Numerical Investigation of Curved Tip Effect on the Performance of 3-D Cavitating Hydrofoils Moving under Free Surface”. In: *Journal of Sailing Technology* 8.01, pp. 39–64. ISSN: 2475-370X. DOI: 10.5957/jst/2023.8.3.39.

Bal, S. (2023b). “The Taper Ratio Influence on the Performance of 3-D Cavitating Hydrofoils Moving under a Free Surface”. In: *Seatific* 3.1, pp. 1–8. DOI: 10.14744/seatific.2023.0001.

Bal, S. and S. A. Kinnas (2002). “A BEM for the Prediction of Free Surface Effects on Cavitating Hydrofoils”. In: *Computational Mechanics* 28.3, pp. 260–274. ISSN: 1432-0924. DOI: 10.1007/s00466-001-0286-7.

Bal, S., S. A. Kinnas, and H. Lee (2001). “Numerical Analysis of 2-D and 3-D Cavitating Hydrofoils Under a Free Surface”. In: *Journal of Ship Research* 45, pp. 34–49. DOI: 10.5957/jsr.2001.45.1.34.

Binns, J. R., P. A. Brandner, and J. Plouhinec (2008). “The Effect of Heel Angle and Free-Surface Proximity on the Performance and Strut Wake of a Moth Sailing Dinghy Rudder T-foil”. In: *The 3rd High Performance Yacht Design Conference*. Auckland, NZ.

Carabineanu, A. (2014). “The Study of the Potential Flow Past a Submerged Hydrofoil by the Complex Boundary Element Method”. In: *Engineering Analysis with Boundary Elements* 39, pp. 23–35. ISSN: 0955-7997. DOI: 10.1016/j.enganabound.2013.10.017.

Chen, Z. (2012). “A Vortex Based Panel Method for Potential Flow Simulation around a Hydrofoil”. In: *Journal of Fluids and Structures* 28, pp. 378–391. ISSN: 0889-9746. DOI: 10.1016/j.jfluidstructs.2011.10.003.

Daskovsky, M. (2000). “The Hydrofoil in Surface Proximity, Theory and Experiment”. In: *Ocean Engineering* 27.10, pp. 1129–1159. ISSN: 00298018. DOI: 10.1016/S0029-8018(99)00032-3.

Duncan, J. H. (1983). “The Breaking and Non-Breaking Wave Resistance of a Two-Dimensional Hydrofoil”. In: *Journal of Fluid Mechanics* 126, pp. 507–520. ISSN: 1469-7645, 0022-1120. DOI: 10.1017/S0022112083000294.

Faltinsen, O. M. (2005). *Hydrodynamics of High-Speed Marine Vehicles*. Cambridge University Press. ISBN: 978-0-521-84568-7.

Filippas, E. S. and K. A. Belibassakis (2014). “Hydrodynamic Analysis of Flapping-Foil Thrusters Operating beneath the Free Surface and in Waves”. In: *Engineering Analysis with Boundary Elements* 41, pp. 47–59. ISSN: 0955-7997. DOI: 10.1016/j.enganabound.2014.01.008.

Giesing, J. P. and A. M. O. Smith (1967). “Potential Flow about Two-Dimensional Hydrofoils”. In: *Journal of Fluid Mechanics* 28.1, pp. 113–129. ISSN: 0022-1120. DOI: 10.1017/S0022112067001934.

Hoque, A., M. Karim, and A. Rahman (2017). “Simulation of Water Wave Generated by Shallowly Submerged Asymmetric Hydrofoil”. In: *Procedia Engineering*. 10th International Conference on Marine Technology, MARTEC 2016 194, pp. 38–43. ISSN: 1877-7058. DOI: 10.1016/j.proeng.2017.08.114.

Hough, G. R. and J. P. Moran (1969). “Froude Number Effects on Two-Dimensional Hydrofoils”. In: *Journal of Ship Research* 13.01, pp. 53–60. ISSN: 0022-4502. DOI: 10.5957/jsr.1969.13.1.53.

Karim, M., B. Prasad, and N. Rahman (2014). “Numerical Simulation of Free Surface Water Wave for the Flow around NACA 0015 Hydrofoil Using the Volume of Fluid (VOF) Method”. In: *Ocean Engineering* 78, pp. 89–94. ISSN: 0029-8018. DOI: 10.1016/j.oceaneng.2013.12.013.

Katz, J. and A. Plotkin (2001). *Low-Speed Aerodynamics*. Cambridge University Press. ISBN: 978-0-521-66552-0.

Kennell, C. and A. Plotkin (1984). “A Second-Order Theory for the Potential Flow About Thin Hydrofoils”. In: *Journal of Ship Research* 28.01, pp. 55–64. ISSN: 0022-4502. DOI: 10.5957/jsr.1984.28.1.55.

Kwag, S. and K. Mori (1991). “Numerical Simulation of Free-Surface Flows around 3-D Submerged Hydrofoil by N-S Solver”. In: *Journal of the Society of Naval Architects of Japan* 1991.170, pp. 93–102. DOI: 10.2534/jjasnaoe1968.1991.170_93.

Laitone, E. V. (1954). “Limiting Pressure on Hydrofoils at Small Submergence Depths”. In: *Journal of Applied Physics* 25.5, pp. 623–626. ISSN: 0021-8979, 1089-7550. DOI: 10.1063/1.1721701.

Michel, W. H., S. F. Hoerner, and L. W. Ward (1954). *Hydrofoil Handbook Volume II - Hydrodynamic Characteristics of Components*. Technical Report. New York 6, NY: Gibbs & Cox, Inc.

Newman, J. N. (2018). *Marine Hydrodynamics*. The MIT Press. ISBN: 978-0-262-53482-6 978-0-262-34499-9.

Ni, Z., M. Dhanak, and T. Su (2021). “Performance of a Hydrofoil Operating Close to a Free Surface over a Range of Angles of Attack”. In: *International Journal of Naval Architecture and Ocean Engineering* 13, pp. 1–11. ISSN: 20926782. DOI: 10.1016/j.ijnaoe.2020.11.002.

Ozdemir, Y. H., T. Cosgun, and B. Barlas (2021). “Wave Field Generated by Finite-Span Hydrofoils Operating beneath a Free Surface”. In: *Brodogradnja: Teorija i praksa brodogradnje i pomorske tehnike* 72.1, pp. 145–167. ISSN: 0007215X, 18455859. DOI: 10.21278/brod72108.

Parkin, B. R., B. Perry, and T. Y. Wu (1955). *Pressure Distribution on a Hydrofoil Running near the Water Surface*. Tech. rep. 47-2. American Institute of Physics.

Patterson, N. and J. Binns (2022). “Development of a Six Degree of Freedom Velocity Prediction Program for the Foiling America’s Cup Vessels”. In: *Journal of Sailing Technology* 7.01, pp. 120–151. ISSN: 2475-370X. DOI: 10.5957/jst/2022.7.6.151.

Perali, P. et al. (2022). “Comparaison de Conditions de Surface Libre Linéarisées Pour l’étude d’un Hydrofoil Submergé à l’aide d’une Approche Potentielle”. In: *25ème Congrès Français de Mécanique*. Nantes, France.

Pernod, L. et al. (2023). “Free-Surface Effects on Two-Dimensional Hydrofoils by RANS-VOF Simulations”. In: *Journal of Sailing Technology* 8.01, pp. 24–38. ISSN: 2475-370X. DOI: 10.5957/jst/2023.8.2.24.

Plotkin, A. (1975). “The Thin-Hydrofoil Thickness Problem Including Leading-Edge Corrections”. In: *Journal of Ship Research* 19.02, pp. 122–129. ISSN: 0022-4502. DOI: 10.5957/jsr.1975.19.2.122.

Prasad, B., T. Hino, and K. Suzuki (2015). “Numerical Simulation of Free Surface Flows around Shallowly Submerged Hydrofoil by OpenFOAM”. In: *Ocean Engineering* 102, pp. 87–94. ISSN: 00298018. DOI: 10.1016/j.oceaneng.2015.04.049.

Speer, T. E. (2001). “The BASILICUS Project - Return of the Cruising Hydrofoil Sailboat”. In: *Chesapeake Sailing Yacht Symposium*. Annapolis, Maryland, USA, pp. 1–22. DOI: 10.5957/CSYS-2001-013.

Thiart, G. D. (1997). “Vortex Lattice Method for a Straight Hydrofoil Near a Free Surface”. In: *International Shipbuilding Progress* 44.437, pp. 5–26. ISSN: 0020-868X. DOI: 10.3233/ISP-1997-4443701.

Thiart, G. D. (2001). “Generalized Vortex Lattice Method for Prediction of Hydrofoil Characteristics”. In: *R&D Journal* 17.2.

Uddin, I. and M. Karim (2017). “Application of Volume of Fluid (VOF) Method for Prediction of Wave Generated by Flow around Cambered Hydrofoil”. In: *Procedia Engineering*. 10th International Conference on Marine Technology, MARTEC 2016 194, pp. 82–89. ISSN: 1877-7058. DOI: 10.1016/j.proeng.2017.08.120.

Wadlin, K. L., C. L. Shuford Jr., and J. R. McGehee (1952). *A Theoretical and Experimental Investigation of the Lift and Drag Characteristics of Hydrofoils at Subcritical and Supercritical Speeds*. Technical Report 1232. Langley Field, Va.: National Advisory Committee for Aeronautics.

Xie, N. and D. Vassalos (2007). “Performance Analysis of 3D Hydrofoil under Free Surface”. In: *Ocean Engineering* 34.8, pp. 1257–1264. ISSN: 0029-8018. DOI: 10.1016/j.oceaneng.2006.05.008.

Yasko, M. (1998). “Boundary Element Method for a Hydrofoil near the Free Surface”. In: *Engineering Analysis with Boundary Elements* 21.2, pp. 191–194. ISSN: 0955-7997. DOI: 10.1016/S0955-7997(98)00010-1.

Yeung, R. W. and Y. C. Bouger (1979). “A Hybrid Integral-Equation Method for Steady Two-Dimensional Ship Waves”. In: *International Journal for Numerical Methods in Engineering* 14.3, pp. 317–336. ISSN: 1097-0207. DOI: 10.1002/nme.1620140303.

Zhu, Q., Y. Liu, and K. P. Y. Dick (2006). “Dynamics of a Three-Dimensional Oscillating Foil Near the Free Surface”. In: *AIAA Journal* 44.12, pp. 2997–3009. ISSN: 0001-1452, 1533-385X. DOI: 10.2514/1.21617.